Atmos. Meas. Tech., 8, 451–461, 2015
www.atmos-meas-tech.net/8/451/2015/
doi:10.5194/amt-8-451-2015

Atmospheric Measurement Techniques
Open Access

Multi-wavelength optical measurement to enhance thermal/optical analysis for carbonaceous aerosol

L.-W. A. Chen[1,2,3], J. C. Chow[2,3], X. L. Wang[2], J. A. Robles[2], B. J. Sumlin[2], D. H. Lowenthal[2], R. Zimmermann[4], and J. G. Watson[2,3]

[1]Department of Environmental and Occupational Health, University of Nevada, Las Vegas, Nevada 89154, USA
[2]Division of Atmospheric Sciences, Desert Research Institute, Reno, Nevada 89512, USA
[3]Key Laboratory of Aerosol Science & Technology, SKLLQG, Institute of Earth Environment, Chinese Academy of Sciences, Xi'an, China
[4]Joint Mass Spectrometry Centre, Chair of Analytical Chemistry, Institute of Chemistry, University of Rostock, Rostock, Germany

Correspondence to: L.-W. A. Chen (antony.chen@unlv.edu)

Received: 22 July 2014 – Published in Atmos. Meas. Tech. Discuss.: 10 September 2014
Revised: 11 December 2014 – Accepted: 13 December 2014 – Published: 27 January 2015

Abstract. A thermal/optical carbon analyzer equipped with seven-wavelength light source/detector (405–980 nm) for monitoring spectral reflectance (R) and transmittance (T) of filter samples allowed "thermal spectral analysis (TSA)" and wavelength (λ)-dependent organic-carbon (OC)–elemental-carbon (EC) measurements. Optical sensing was calibrated with transfer standards traceable to absolute R and T measurements, adjusted for loading effects to report spectral light absorption (as absorption optical depth ($\tau_{a,\lambda}$)), and verified using diesel exhaust samples. Tests on ambient and source samples show OC and EC concentrations equivalent to those from conventional carbon analysis when based on the same wavelength ($\sim$ 635 nm) for pyrolysis adjustment. TSA provides additional information that evaluates black-carbon (BC) and brown-carbon (BrC) contributions and their optical properties in the near infrared to the near ultraviolet parts of the solar spectrum. The enhanced carbon analyzer can add value to current aerosol monitoring programs and provide insight into more accurate OC and EC measurements for climate, visibility, or health studies.

1 Introduction

Thermal/optical analysis (TOA) quantifies particulate-matter (PM) organic carbon (OC) and elemental carbon (EC) collected on quartz-fiber filters (Watson et al., 2005; Cao et al., 2007; Bougiatioti et al., 2013). TOA based on the IMPROVE_A protocol (Chow et al., 2007a, 2011) has determined OC and EC concentrations in tens of thousands of samples each year from long-term chemical speciation networks operated in the US (IMPROVE, 2014; U.S.EPA, 2014), Canada (Dabek-Zlotorzynska et al., 2011), and China (Zhang et al., 2012). IMPROVE_A specifies stepped heating up to 580 °C in an inert helium (He) atmosphere (> 99.99 % purity), where most organic compounds are either evaporated or decomposed (Chow et al., 1993), followed by a second stage of stepped heating to 840 °C in 98 % He / 2 % O_2 to remove EC on the filter. Since some of the OC is converted to EC through pyrolysis in pure He, as evidenced by darkening of the filter, IMPROVE_A also specifies a reflectance pyrolysis adjustment. Reflected light at wavelength $\lambda = 633$ nm is monitored throughout the heating (Huntzicker et al., 1982). OC and EC are defined as carbon evolved before and after the filter reflectance (R) returns to its initial level, respectively.

In addition to reflectance, some TOA protocols use transmitted light (T) to monitor the pyrolysis (Birch and Cary, 1996; Turpin et al., 1990). ECs based on R or T splits are referred to as ECR and ECT, respectively. In addition to particle deposits, adsorbed organic vapors within the quartz-fiber filter (Chow et al., 2010; Watson et al., 2009) can pyrolyze during the analysis (Yang and Yu, 2002; Chow et al., 2004). ECR differs from ECT since the R signal is dominated by pyrolyzed OC (POC) on the filter surface, while the T sig-

nal is influenced by POC both on and within the filter (Chen et al., 2004; Chow et al., 2004). Unlike IMPROVE_A, which reports both ECR and ECT, other TOA protocols employ different temperature steps, often reporting only the ECT results (Birch and Cary, 1996; Cavalli et al., 2010; NIOSH, 1999; Schauer et al., 2003; Peterson and Richards, 2002).

The R and/or T measurements as part of TOA can infer the light absorption coefficient (b_{abs}), analogous to the principle of optical absorption monitors such as the aethalometer (Hansen et al., 1984), particle-soot absorption photometer (PSAP; Bond et al., 1999), and the multi-angle absorption photometer (MAAP; Petzold and Schönlinner, 2004). Both the aethalometer and PSAP apply T attenuation, while the MAAP incorporates both R and T attenuations in the calculation of b_{abs}. In any case, it is necessary to compensate for multiple-scattering and loading effects of the particle-filter matrix that cause deviations from the simple Beer's law (Chen et al., 2004; Arnott et al., 2005b; Virkkula et al., 2005). Black-carbon (BC) concentrations can be derived from b_{abs} by applying a mass- and wavelength-specific absorption efficiency (MAE_λ, typically in $m^2\,g^{-1}$). Many collocated measurements show high correlations but different slopes in BC/EC comparisons (Ahmed et al., 2009; Quincey et al., 2009; Reisinger et al., 2008; Snyder and Schauer, 2007; Chow et al., 2009). This confirms the overlapping concept of EC and BC but also signifies the complex nature of carbonaceous material and uncertainties in such measurements (Andreae and Gelencséer, 2006; Moosmüller et al., 2009; Petzold et al., 2013; Lack et al., 2014).

While BC (or EC) absorbs light strongly across the solar spectrum (300–1000 nm), some organic compounds that evolve in the OC step can also absorb light, especially at shorter wavelengths (< 600 nm). These compounds have been termed "brown carbon" (BrC) and are associated with the smoldering phase of biomass burning and some end products of secondary aerosol formation (Andreae and Gelencsér, 2006; Clarke et al., 2007; Zhang et al., 2011). The spectral dependence of b_{abs} is often described by α:

$$\alpha(\lambda) = -\frac{\mathrm{dln}(b_{abs}(\lambda))}{\mathrm{dln}(\lambda)}, \quad (1)$$

where $\alpha(\lambda)$ is the absorption Ångström exponent. For BC (or EC) with graphitic-like structure and a constant refractive index, $\alpha = 1$ and b_{abs} is proportional to λ^{-1}. For BrC and mineral dust, α varies with λ and is mostly > 1 (Moosmüller et al., 2009; Chen et al., 2015), causing b_{abs} to increase more rapidly towards shorter wavelengths (blue and ultraviolet) than is the case for BC. The aerosol deposit thus appears to be brown – or sometimes yellow, red, or chartreuse – as the longer wavelengths of illuminating light are reflected and the shorter wavelengths are absorbed. The multi-wavelength aethalometer has revealed different spectral patterns that are indicative of BC, BrC, dust, and their mixtures (Sandradewi et al., 2008; Favez et al., 2009; Yang et al., 2009).

Given the large number of samples per year analyzed by TOA worldwide, the optical data acquired as part of the analysis could be used, in addition to OC and EC, for studies relevant to source apportionment, human health, visibility, and climate. Described and characterized here is a retrofit of a TOA carbon analyzer that expands the single-wavelength R and T monitoring to seven wavelengths for the IMPROVE_A analysis, hereafter designated thermal spectral analysis (TSA). Equivalence of the OC and EC fractions from TOA and TSA is demonstrated for several source and receptor samples, and the wavelength dependence of the OC–EC split is investigated. An approach to report spectral b_{abs} (as absorption optical depth) and α for decoupling the BC and non-BC components is also introduced. As an aid to readers, all abbreviations used in this paper are listed in the Supplement (Table S1).

2 Instrument design and calibration

The 633 nm He/neon (Ne) laser in the DRI Model 2001 carbon analyzer (Chow et al., 2011; Chen et al., 2012) is replaced with a package of seven diode lasers with wavelengths (λ) of 405, 450, 532, 635, 780, 808, and 980 nm. The use of diode lasers substantially reduces the cost of the optical module. It also provides stronger signals than using a light-emitting diode (LED) in other designs (e.g., Hadley et al., 2008), despite being limited by the wavelengths commercially available. While the 635 nm approximates the He/Ne laser, other wavelengths were selected to cover the visible and near-infrared regions. The lasers are alternately pulsed (2 consecutive pulses per laser, 14 pulses per cycle) and lock-in amplified at a frequency of 30 Hz, resulting in two cycles and $\sim$ four pulses for each wavelength every second. The bifurcated fiber optic for delivering the He / Ne laser to the reflectance light pipe is replaced with an eight-furcated optical-fiber bundle, one for each of the lasers and the last for transferring the light reflected from the filter punch (0.5 cm^2) to a photodiode (Fig. 1). Another light pipe on the opposite side of the filter directs the transmitted light toward a separate photodiode detector.

Photodiode signals are acquired with an NI6216 data acquisition system (National Instruments, Austin, TX) at a rate of up to 100 000 data points per second. The system integrates the product of photodiode and reference (30 Hz square wave) signals every second to suppress noise (e.g., from 60 Hz power supply and oven glow, random noise, and baseline drift). The resulting integrals are reported as the spectral laser reflectance and transmittance (LR_λ and LT_λ, respectively). Example thermograms with LR_λ and LT_λ are illustrated in Fig. S1 of the Supplement.

LR_λ and LT_λ are relative terms depending on not only the optical properties of the sample but also laser intensity, the geometry of the laser/detector setup, and the response of the photodiode. They are related to absolute fil-

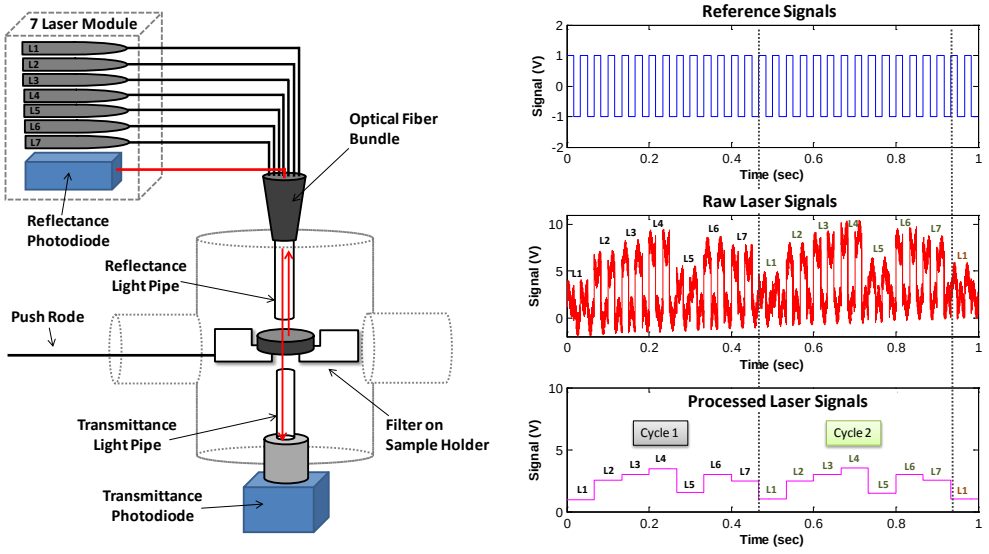

Figure 1. Configuration of optical sensing (left) modified from the DRI Model 2001 analyzer (Chen et al., 2012). The seven-laser module (i.e., L1-L7) represents seven diode lasers with wavelengths of 405, 450, 532, 635, 780, 808, and 980 nm. Reference (top right) and laser (middle right) signals are modulated at 30 Hz for a lock-in amplification of the reflectance or transmittance signals (bottom right). Only 30 Hz signals with the same phase as the reference are amplified at gains proportional to the reference signal voltage and number of data points integrated.

ter reflectance and transmittance (FR_λ and FT_λ, i.e., fraction of light reflected from or transmitted through the filter, respectively), using a set of transfer standards consisting of eight $PM_{2.5}$ quartz-fiber filters acquired using high-volume samplers from the Fresno Supersite (Watson et al., 2000; Chow et al., 2009), with EC loadings ranging from 0.9 to 15.8 $\mu g\,cm^{-2}$ (Fig. S2). The high-volume filters (406 cm^2) represent well-characterized urban aerosol, while providing sufficient sample for extensive testing. FR_λ and FT_λ of the transfer standards were predetermined using an integrating-sphere spectrometer (Lambda 35, Perkin Elmer, Massachusetts, USA; see, e.g., Zhong and Jang, 2011; Chen et al., 2015) traceable to NIST (National Institute of Standard and Technology) standards for wavelengths between 300 and 1000 nm.

Figure 2 compares LR_λ and LT_λ with FR_λ and FT_λ, respectively, for the transfer standards. Within the range of FR_λ (0.1–0.8) and FT_λ (0.0001–0.1), highly significant linear relationships ($r^2 > 0.9$) demonstrate the stability of the LR_λ and LT_λ measurements and the feasibility of converting them to FR_λ and FT_λ through calibration with a standardized spectrometer. Figure S1 illustrates the changes in FR_λ and FT_λ, retrieved from LR_λ and LT_λ, throughout a typical TSA. The uncertainty of the FR_λ and FT_λ retrievals may be evaluated by the coefficient of variance of the root mean square residual (CV-RMSR) in the FR_λ / LR_λ and FT_λ / LT_λ regression, respectively:

$$\text{CV-RMSR} = \frac{1}{\overline{Y_{\text{obs}}}}\sqrt{\frac{\sum(Y_{\text{cal}} - Y_{\text{obs}})^2}{n-2}}, \quad (2)$$

where Y_{obs} is the FR_λ or FT_λ measured by the integrating-sphere spectrometer, Y_{cal} is the FR_λ or FT_λ calculated from LR_λ or LT_λ, respectively, and n is the number of samples. $FR_{633\text{ nm}}$ and $FT_{633\text{ nm}}$ based on the He / Ne laser of a typical Model 2001 analyzer exhibit a ~ 3 % uncertainty (Fig. 2). For this retrofit, FR_λ uncertainties range from 3 to 11 % and FT_λ uncertainties range from 5 to 18 %, with the best precision shown at 450 and 808 nm. The divergence in uncertainty is attributed to the quality of the laser and the sensitivity of the photodiode detector for different wavelengths. Ongoing efforts to improve the signal-to-noise ratio of R and T measurements by using different lasers and averaging algorithms will be documented in subsequent papers.

3 Consistency of the OC–EC split

Several source and ambient $PM_{2.5}$ samples (Table 1) are used for testing the system. Samples from the Fresno Supersite (2 April 2003–28 December 2003) contain a mixture of carbonaceous materials from fresh engine exhaust, biomass burning, and cooking (Chen et al., 2007; Chow et al., 2007b; Gorin et al., 2006; Schauer and Cass, 2000). Reno ambient samples were acquired during the period of Rim Fire (17 August 2013–24 October 2013) and are dominated by an aged biomass burning plume containing mixed flaming and smoldering emissions. Source testing as part of the Lake Tahoe Prescribed Burning Study (Malamakal et al., 2013) and Gasoline/Diesel Split Study (Fujita et al., 2007) provided pure biomass burning and diesel exhaust samples, respec-

Table 1. Comparison of TC, OCR, OCT, ECR, and ECT between the 633 nm (TOA) and 635 nm (TSA) optical splits following the IMPROVE_A protocol.[a]

Sample type	Optical split (nm)[b]		Sample no. and avg.[c]			Corr.	Deming regression: $y = m \times x + b$		RD: $2(y-x)/(y+x)$	
	x	y	n	x	y	r^2	m[c] ($\pm 1\sigma$[d])	b[c] ($\pm 1\sigma$[d])	mean $\pm 1\sigma$	p[e]
TC										
Fresno Supersite	635	633	10	20.30	20.05	1.00	0.97 ± 0.05	0.38 ± 0.75	-0.01 ± 0.04	0.56
Reno wildfire	635	633	14	30.69	30.21	1.00	0.91 ± 0.06	2.14 ± 1.18	0.04 ± 0.09	0.15
Prescribed burn	635	633	9	19.27	20.11	1.00	1.06 ± 0.09	-0.32 ± 1.12	0.01 ± 0.14	0.91
Diesel exhaust	635	633	11	8.10	7.78	0.97	0.99 ± 0.05	-0.26 ± 0.48	-0.06 ± 0.15	0.21
All	635	633	44	20.34	20.23	0.99	0.95 ± 0.07	0.89 ± 1.00	0.00 ± 0.12	0.85
OCR										
Fresno Supersite	635	633	10	16.02	15.91	0.99	0.97 ± 0.06	0.44 ± 0.76	0.00 ± 0.05	0.85
Reno wildfire	635	633	14	27.62	26.99	1.00	0.90 ± 0.07	2.09 ± 1.27	0.03 ± 0.09	0.30
Prescribed burn	635	633	9	17.22	18.25	1.00	1.07 ± 0.06	-0.12 ± 0.76	0.03 ± 0.13	0.65
Diesel exhaust	635	633	11	4.08	3.91	0.52	0.95 ± 0.35	0.04 ± 1.35	-0.04 ± 0.17	0.46
All	635	633	44	16.97	16.91	0.99	0.94 ± 0.08	0.90 ± 0.99	0.00 ± 0.12	0.68
OCT										
Fresno Supersite	635	633	10	17.80	17.82	1.00	1.01 ± 0.03	-0.17 ± 0.43	0.00 ± 0.04	0.85
Reno wildfire	635	633	14	29.07	28.64	1.00	0.92 ± 0.06	1.93 ± 1.19	0.03 ± 0.08	0.14
Prescribed burn	635	633	9	18.11	18.92	1.00	1.07 ± 0.05	-0.37 ± 0.72	0.01 ± 0.13	0.65
Diesel exhaust	635	633	11	4.42	4.14	0.46	1.01 ± 0.46	-0.33 ± 1.91	-0.07 ± 0.20	0.32
All	635	633	44	18.10	18.07	0.99	0.96 ± 0.07	0.74 ± 0.94	-0.01 ± 0.13	0.75
ECR										
Fresno Supersite	635	633	10	4.28	4.15	1.00	0.99 ± 0.06	-0.11 ± 0.17	-0.06 ± 0.08	0.06
Reno wildfire	635	633	14	3.07	3.22	0.99	1.04 ± 0.07	0.02 ± 0.15	0.12 ± 0.23	0.14
Prescribed burn	635	633	9	2.05	1.86	0.88	0.92 ± 0.18	-0.03 ± 0.34	-0.13 ± 0.25	0.25
Diesel exhaust	635	633	11	4.02	3.87	0.99	0.97 ± 0.07	-0.03 ± 0.23	-0.17 ± 0.30	0.12
All	635	633	44	3.37	3.31	0.99	1.00 ± 0.03	-0.05 ± 0.08	-0.04 ± 0.25	0.17
ECT										
Fresno Supersite	635	633	10	2.50	2.23	0.99	0.78 ± 0.12	0.29 ± 0.22	-0.07 ± 0.14	0.13
Reno wildfire	635	633	14	1.62	1.57	0.98	0.82 ± 0.02	0.24 ± 0.07	0.10 ± 0.30	0.33
Prescribed burn	635	633	9	1.16	1.18	0.85	0.87 ± 0.10	0.17 ± 0.13	0.07 ± 0.30	0.50
Diesel exhaust	635	633	11	3.68	3.64	0.99	0.92 ± 0.13	0.24 ± 0.30	-0.08 ± 0.33	0.70
All	635	633	44	2.24	2.16	0.98	0.90 ± 0.03	0.14 ± 0.06	0.01 ± 0.28	0.74

[a] TC: total carbon; OCR: organic carbon by reflectance; OCT: organic carbon by transmittance; ECR: elemental carbon by reflectance; and ECT: elemental carbon by transmittance following the IMPROVE_A thermal/optical carbon analysis protocol (Chow et al., 2007a). TOA: thermal/optical analyses; TSA: thermal/spectral analyses. [b] x is by retrofitted seven-wavelength carbon analyzer; y is by conventional single-wavelength (633 nm) DRI Model 2001 thermal/optical carbon analyzer. [c] Concentration in $\mu g\,cm^{-2}$; m is the slope; b is the intercept in $\mu g\,cm^{-2}$. [d] σ: standard deviation. [e] Student's t test p values.

tively. All these samples were analyzed by both TSA (using the retrofit) and TOA (using conventional Model 2001 analyzers) following the IMPROVE_A protocol.

Table 1 compares total carbon (TC), OC, and EC by reflectance (i.e., OCR and ECR) and transmittance (i.e., OCT and ECT) between TSA with the 635 nm and TOA with the normal 633 nm OC–EC split. As expected, TC is equivalent, with the averages agreeing within $\pm$ 5 % and regression slopes (m) ranging from 0.91 and 1.06 for each of the four sample types. The relative difference (RD), defined as the ratio of the difference divided by the average of two measurements (i.e., TSA and TOA) on the same sample, does not differ from 0 at the 5 % significance level ($p > 0.05$). The standard deviations of RD, a measure of random error, are higher for source (14–15 %) than for ambient (4–9 %) samples, indicative of greater deposit inhomogeneity for these samples, possibly due to variable sampling conditions over short sampling durations.

TSA and TOA also yield statistically equivalent OC and EC results, either by R or T (Table 1). Figure 3 visualizes the comparisons. With respect to the standard deviation of RD, OCR and OCT are similar to TC, while ECR and ECT are higher (up to 33 %) due to a lower fraction of EC in TC. By category average, ECR and ECT account for 10–50 and 5–46 % of TC, respectively. In general, ECR > ECT, as reported in previous studies (Khan et al., 2012; Han et al., 2013; Chow

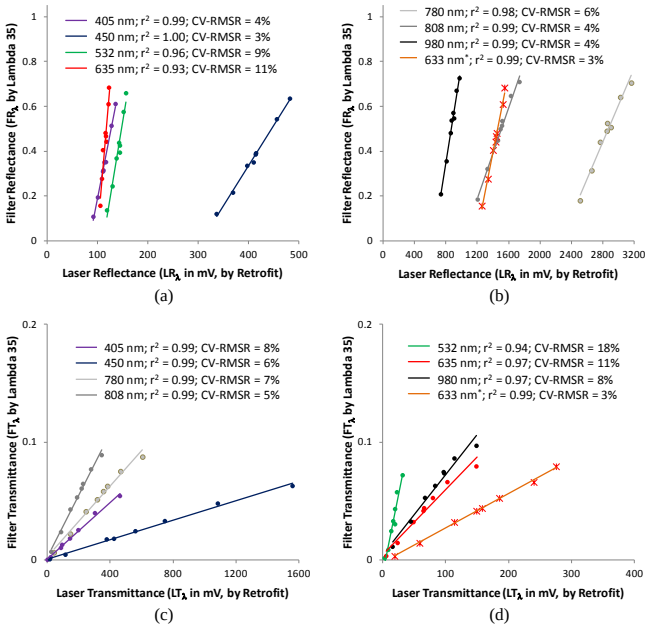

Figure 2. Calibration of spectral laser **(a, b)** reflectance and **(c, d)** transmittance measurements (LR_λ and LT_λ, respectively, in millivolts (mV)) from the retrofitted seven-wavelength carbon analyzer at room temperature against absolute filter reflectance and transmittance (FR_λ and FT_λ, respectively) quantified by the Lambda integrating-sphere spectrometer, using eight Fresno ambient samples (5/6, 6/6, 6/19, 7/3, 9/29, 11/4, 11/13, and 12/28 of 2003) of various loadings as transfer standards. The 633 nm data are from a conventional carbon analyzer. r^2 and CV-RMSR evaluate the regression performance.

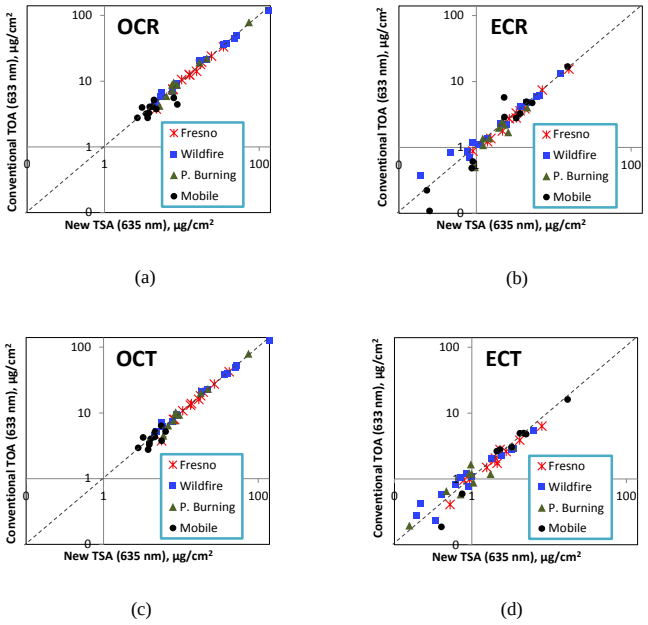

Figure 3. Comparison of organic and elemental carbon by reflectance optical correction (i.e., OCR and ECR, respectively) between the conventional thermal/optical analysis (TOA based on 633 nm optical split) and seven-wavelength thermal/spectral analysis (TSA based on 635 nm optical split) following the IMPROVE_A protocol. Note that x and y axes are on log scales.

et al., 2001; Schmid et al., 2001), consistent with organic vapors pyrolyzed within the filter leaving the sample after native EC and POC in the surface deposit have evolved (Chen et al., 2004). POC was least apparent for the diesel exhaust samples where optical adjustments were negligible.

The basic assumptions for optical adjustment include the following: (1) OC does not absorb light and (2) POC has the same apparent MAE as EC. Within-the-filter POC shows no apparent MAE by R (i.e., cannot detect it for any wavelengths) but high MAEs by T (higher than EC due to a multiple-scattering effect (Chow et al., 2004; Subramanian et al., 2006)). This leads to divergent ECR and ECT results. Since the multiple-scattering effect is larger for shorter wavelengths, ECT is expected to decrease with the wavelength at which the split is made. On the other hand, Chow et al. (1993) observed that the operational definition for EC by any TOA protocol might contain some light-absorbing OC. BrC, if present, would lower the baselines of R and T (prior to thermal analysis) for shorter wavelengths, resulting in earlier split points and larger EC reported than that from longer wavelengths.

Table 2 compares OC–EC splits for 635 nm with splits derived from shorter (450 nm) and longer (808 nm) wavelengths that have the lowest LR or LT uncertainties. ECRs based on the 635 nm split agree well with those based on the 808 nm split (i.e., slopes within the standard error from unity and $p(\mathrm{RD}) > 0.02$) for all the sample types. This demonstrates that the 633 nm R split commonly used for optical adjustment since Huntzicker et al. (1982) does not significantly respond to BrC absorption compared with longer visible or infrared wavelengths. For ECT, the 880 nm split yielded higher values than the 635 nm split, especially for biomass-burning-dominated samples. This is consistent with ECT being influenced by POC within the filter and decreasing ECT with decreasing wavelength.

The 450 nm split appears to be sensitive to BrC content, as evidenced by larger ECR than those determined with 635 nm (except for diesel exhaust samples, where BrC contents are low). The difference is largest for the aged Reno wildfire samples, which may also contain some secondary organic aerosol formed during transport over the 200 km distance between Yosemite National Park and Reno, Nevada. As demonstrated in Fig. S1, shorter wavelengths produce earlier splits, resulting in higher ECR concentrations. The increase of ECT due to a 450 nm optical correction is not evident, which may be due to the opposing effects of BrC and POC at the shorter wavelength.

Table 2. Comparison of TSA-determined 635 nm ECR and ECT with 880 nm and 450 nm following the IMPROVE_A protocol.

Sample type	Optical split (nm)[a]		Sample no. and avg.[b]			Corr.	Deming regression: $y = m \times x + b$		RD: $2(y-x)/(y+x)$	
	x	y	n	x	y	r^2	m[b]($\pm1\sigma$[c])	b[b]($\pm1\sigma$[c])	mean$\pm$ 1σ	p[d]
ECR										
Fresno Supersite	635	450	10	4.28	4.74	1.00	1.23 ± 0.04	-0.55 ± 0.13	0.01 ± 0.13	0.82
Reno wildfire	635	450	14	3.07	4.29	0.95	1.90 ± 0.58	-1.55 ± 1.24	0.14 ± 0.25	0.06
Prescribed burn	635	450	9	2.05	2.14	0.98	1.41 ± 0.23	-0.74 ± 0.39	-0.03 ± 0.16	0.57
Diesel exhaust	635	450	11	4.02	3.93	1.00	1.00 ± 0.01	-0.10 ± 0.06	-0.08 ± 0.11	0.06
All	635	450	44	3.37	3.86	0.90	1.36 ± 0.28	-0.71 ± 0.66	0.02 ± 0.19	0.76
Fresno Supersite	635	808	10	4.28	4.12	1.00	0.95 ± 0.08	0.06 ± 0.22	-0.05 ± 0.05	0.03
Reno wildfire	635	808	14	3.07	3.22	1.00	1.04 ± 0.08	0.03 ± 0.17	0.15 ± 0.23	0.02
Prescribed burn	635	808	9	2.05	2.12	0.99	1.00 ± 0.09	0.06 ± 0.17	0.03 ± 0.09	0.30
Diesel exhaust	635	808	11	4.02	4.00	1.00	1.00 ± 0.00	-0.02 ± 0.02	-0.01 ± 0.02	1.00
All	635	808	44	3.37	3.40	1.00	0.99 ± 0.03	0.05 ± 0.07	0.04 ± 0.16	0.19
ECT										
Fresno Supersite	635	450	10	2.50	2.44	1.00	1.00 ± 0.02	-0.05 ± 0.07	-0.04 ± 0.08	0.16
Reno wildfire	635	450	14	1.62	1.35	0.99	0.85 ± 0.06	-0.02 ± 0.06	-0.20 ± 0.14	0.00
Prescribed burn	635	450	9	1.16	1.07	0.98	1.06 ± 0.25	-0.16 ± 0.22	-0.08 ± 0.24	0.16
Diesel exhaust	635	450	11	3.68	3.59	1.00	0.97 ± 0.01	0.01 ± 0.04	-0.04 ± 0.06	0.07
All	635	450	44	2.24	2.10	0.99	0.97 ± 0.02	-0.08 ± 0.03	-0.10 ± 0.16	0.00
Fresno Supersite	635	808	10	2.50	2.67	1.00	1.03 ± 0.04	0.10 ± 0.08	0.08 ± 0.04	0.00
Reno wildfire	635	808	14	1.62	2.00	0.99	1.24 ± 0.04	-0.01 ± 0.08	0.18 ± 0.18	0.00
Prescribed burn	635	808	9	1.16	1.27	0.99	1.10 ± 0.12	-0.01 ± 0.12	-0.09 ± 0.60	0.13
Diesel exhaust	635	808	11	3.68	3.53	1.00	0.99 ± 0.01	-0.11 ± 0.07	-0.24 ± 0.41	0.01
All	635	808	44	2.24	2.38	0.99	1.01 ± 0.07	0.11 ± 0.12	0.00 ± 0.38	0.02

[a] x and y are both by modified seven-wavelength carbon analyzer but with optical pyrolysis adjustment at different wavelengths. [b] Concentration in $\mu g\,cm^{-2}$; m is the slope; b is the intercept in $\mu g\,cm^{-2}$. [c] σ: standard deviation. [e] Student's t test p values.

4 Multi-wavelength absorption retrieval

Light absorption by particles on the filter is often estimated by transmittance attenuation (ATN):

$$\mathrm{ATN}_\lambda = -\ln\left(\frac{\mathrm{FT}_{\lambda,\mathrm{i}}}{\mathrm{FT}_{\lambda,\mathrm{f}}}\right), \quad (3)$$

where i and f indicate FT_λ measured before and after thermal analysis, respectively. $\mathrm{FT}_{\lambda,f}$ approximates a blank filter since all of the carbon has been removed. ATN_λ includes scattering and absorption within the substrate. On the other hand, the absorption optical depth ($\tau_{\mathrm{a},\lambda}$) measures only the light absorption. For diesel soot samples with negligible BrC and POC,

$$\tau_{\mathrm{a},\lambda} = \mathrm{MAE}_{\lambda,\mathrm{EC}} \times [\mathrm{EC}], \quad (4)$$

where [EC] is the areal concentration of EC on filter in $\mu g\,cm^{-2}$. If there were no filter effects, ATN and τ_a would be identical for a given λ as described by Beer's law. With the knowledge of sampling volume (V) and filter area (A), ambient b_abs can be calculated from $\tau_\mathrm{a} \times A/V$.

The relationship of [EC] and $\mathrm{ATN}_{635\ \mathrm{nm}}$ throughout the EC2 step (740 °C in a 98 % He / 2 % O_2 atmosphere) of the IMPROVE_A analysis for a diesel exhaust sample is shown in Fig. 4. Since in this case carbon evolved during EC2 is exclusively EC, the temporal variation in [EC], i.e., d[EC] / dt, can be determined from carbon released and detected by the carbon analyzer. Arnott et al. (2005b) proposed a quadratic relationship between [EC] and ATN, derived from

$$\frac{\mathrm{dATN}_\lambda}{\mathrm{dt}} = \frac{M_\lambda \times \mathrm{MAE}_{\lambda,\mathrm{EC}}}{\sqrt{1+\beta_\lambda \times [\mathrm{EC}]}} \times \frac{\mathrm{d[EC]}}{\mathrm{d}t} \quad (5)$$

and thus

$$[\mathrm{EC}] = \frac{\beta_\lambda}{4(M_\lambda \times \mathrm{MAE}_{\lambda,\mathrm{EC}})^2}\mathrm{ATN}_\lambda{}^2 + \frac{1}{M_\lambda \times \mathrm{MAE}_{\lambda,\mathrm{EC}}}\mathrm{ATN}_\lambda, \quad (6)$$

where M_λ and β_λ account for the wavelength-specific multiple-scattering and loading effects, respectively. Eq. (6) fits the relationship in Fig. 4 well ($r^2 > 0.99$), thereby allowing M_λ and β_λ to be estimated. EC (quantified by IMPROVE_A ECR or ECT) of all the diesel exhaust samples exhibits a consistent dependence on the initial sample $\mathrm{ATN}_{635\ \mathrm{nm}}$ (prior to TSA) (Fig. 4). This supports the use of $\mathrm{ATN}_{635\ \mathrm{nm}}$ as a surrogate for EC and light absorption. Simi-

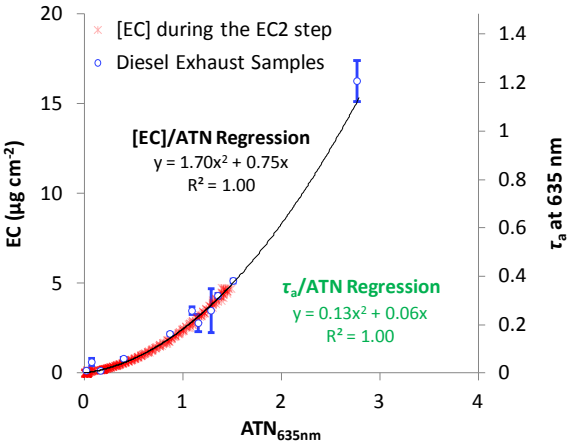

Figure 4. Relationship of EC concentration, [EC], versus $ATN_{635\ nm}$ from all 1 s measurements during the EC2 step (740 °C in a 98 % He / 2 % O_2 atmosphere) of IMPROVE_A analysis for a diesel exhaust sample (CIFQ074 from the Gas/Diesel Split Study (Fujita et al., 2007)). Also shown are paired [EC]–$ATN_{635\ nm}$ of 11 diesel exhaust samples, where EC is determined from IMPROVE_A and $ATN_{635\ nm}$ from initial filter transmittance. Circles and error bars indicate the average and spread, respectively, of EC by transmittance and reflectance (i.e., ECT and ECR, respectively). $\tau_{a,635\ nm}$ was further calculated from a MAE of 7.4 $m^2\ g^{-1}$ × [EC], and the regression result between $\tau_{a,635\ nm}$ and $ATN_{635\ nm}$ is shown in green.

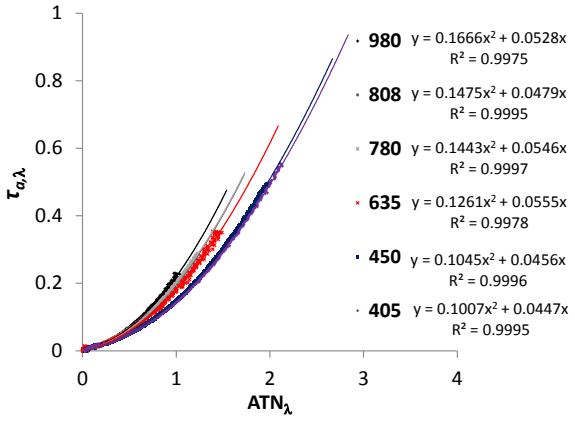

Figure 5. $\tau_{a,\lambda}$–ATN_{λ} relationships for 405–980 nm wavelengths, based on a diesel exhaust reference sample. Results for 532 nm are not shown owing to lack of sufficient detector signal-to-noise ratio at this wavelength.

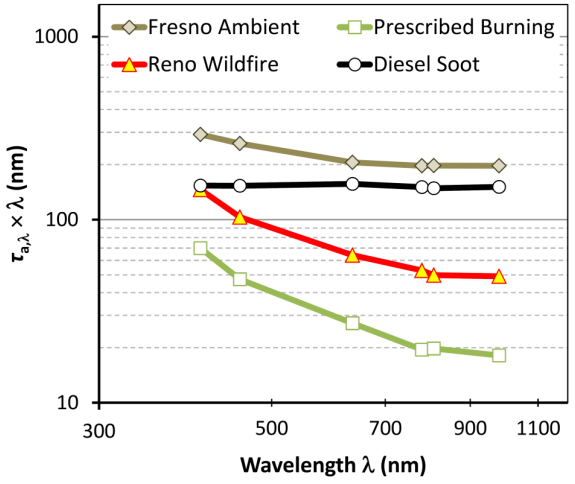

Figure 6. Product of absorption optical depth ($\tau_{a,\lambda}$) and wavelength (λ) as a function of λ by sample type. $\tau_{a,\lambda}$ shown represents averages over each of the sample types.

lar relationships hold between [EC] and ATN for other wavelengths (Fig. S3). The largest scatter observed for 532 nm corresponds to the highest uncertainty in $FT_{532\ nm}$ retrievals; it results from the slow laser response time to modulation and the low sensitivity of the transmittance photodiode detector at this wavelength, which will be addressed in a subsequent design of the retrofit optics.

To relate $\tau_{a,635\ nm}$ to $ATN_{635\ nm}$, a MAE (EC) of 7.4 $m^2\ g^{-1}$ at 635 nm was used. The MAE was derived from concurrent b_{abs}, by a photoacoustic sensor at 1047 nm, and EC, by IMPROVE_A, measurements during the Gasoline/Diesel Split Study (Arnott et al., 2005a) and assuming an α of 1 in Eq. (1). The quadratic relationship holds for all of the available wavelengths, as seen in Fig. 5. Light absorption is enhanced by the filter since any $\tau_{a,\lambda} < 1$ corresponds to a larger ATN_{λ}, with more amplification towards shorter wavelengths. These $\tau_{a,\lambda}$–ATN_{λ} relationships would apply to any samples, regardless of the nature of light-absorbing material (e.g., EC, BC, BrC, or mineral dust). Particle penetration depth and, to a lesser degree, single-scattering albedo and the asymmetry g factor can influence the $\tau_{a,\lambda}$–ATN_{λ} dependence, though for a similar sampling configuration and filter material/thickness with typical loading, the perturbation is expected to be small (Chen et al., 2004; Arnott et al., 2005b). Retrieval algorithms employing both R and T such as those in Petzold and Schönlinner (2004) should be developed in the future to utilize all the information available.

Using the relationships in Fig. 5, $\tau_{a,\lambda}$ was calculated for all samples from the initially measured ATN_{λ} values, with the average $\tau_{a,\lambda} \times \lambda$ by sample type compared in Fig. 6. The nearly constant $\tau_{a,\lambda} \times \lambda$ for diesel exhaust samples, i.e., $\tau_{a,\lambda} \propto \lambda^{-1}$, is consistent with the exclusive contribution of EC to light absorption. BC derived from the $\tau_{a,\lambda}$ would be equivalent to diesel EC. Averaged $\tau_{a,\lambda} \times \lambda$ increases by factors of 1.5, 3.0, and 3.9 from 980 to 405 nm for the Fresno ambient, Reno wildfire, and prescribed-burning samples, respectively. This reflects different levels of non-EC contribution.

Table 3. Average $\tau_{a,635\ nm}$ for four sample types and their respective BC and BrC fractions, BrC absorption Ångström exponent, and diesel-EC-equivalent BC (BC_d) concentration. IMPROVE_A ECR and ECT determined by the 635 nm optical adjustment are compared to BC_d in terms of average and p value of the relative difference (RD).

Sample type	$\tau_{a,635\ nm}$	$\tau_{a,635\ nm,BC}$	$\tau_{a,635\ nm,BrC}$ (% in τ_a)	α_{BC}^a	α_{BrC}	BC_d^b ($\mu g\ cm^{-2}$)	ECR ($\mu g\ cm^{-2}$)	ECT ($\mu g\ cm^{-2}$)	p value ($RD_{BC,ECR}$)	p value ($RD_{BC,ECT}$)
Fresno (ambient)	0.33	0.30	0.03 (10 %)	1	4.8 ± 1.5	4.0	4.3	2.5	0.02	0.87
Reno (wildfire)	0.10	0.07	0.02 (26 %)	1	4.8 ± 1.7	1.0	3.1	1.6	0.00	0.00
Prescribed burning	0.04	0.02	0.02 (46 %)	1	4.2 ± 1.8	0.3	2.1	1.2	0.00	0.00
Diesel exhausts	0.26	0.26	0.00 (1 %)	1	2.3 ± 0.1	3.5	4.0	3.7	0.05	0.06

[a] Pre-assumed values. [b] Calculated from $\tau_{a,635\ nm,BC}/(7.4\ m^2\ g^{-1})$.

5 Separation of BC and BrC contributions

A simplified two-component model consisting of BC and BrC, each with explicit absorption Ångström exponents (α_{BC} and α_{BrC}), is used to explain the spectral dependence of $\tau_{a,\lambda}$ in the samples:

$$\lambda_{a,\lambda} = q_{BC} \times \lambda^{-\alpha_{BC}} + q_{BrC} \times \lambda^{-\alpha_{BrC}}, \quad (7)$$

where q_{BC} and q_{BrC} are fitting coefficients. This is analogous to the approach of Sandradewi et al. (2008), who considered the two components to be traffic and wood-burning particles and Hadley et al. (2008), who modeled two components of BC and char. Assuming an α_{BC} of 1 the same as diesel EC, then

$$\tau_{a,\lambda} \times \lambda = q_{BC} + q_{BrC} \times \lambda^{-(\alpha_{BrC}-1)}. \quad (8)$$

Fitting coefficients in Eq. (8) were obtained for α_{BrC} values between 2 and 8 by least-square linear regression, and the α_{BrC} that led to the overall best fit in terms of r^2 was selected as the effective absorption Ångström exponent of BrC with which $\tau_{a,\lambda,BC}$ and $\tau_{a,\lambda,BrC}$ can be calculated from the first and second terms of Eq. (7). This fitting takes advantage of all six wavelengths. For each of the 44 samples, Fig. S4 shows that fitted $\tau_{a,\lambda}$ are within ±5 % of the measured values for $\tau_{a,\lambda} > 0.01$. Examples of the $\tau_{a,\lambda}$ decomposition as a function of wavelength are shown in Fig. S5.

Table 3 summarizes the apportionment of $\tau_{a,635\ nm}$ into BC and BrC fractions along with average α_{BrC}, "diesel-EC-equivalent" BC (termed BC_d hereafter), ECR, and ECT by sample type. Consistent with Fig. 5, BrC contributions to $\tau_{a,635\ nm}$ are much higher in prescribed burning than in diesel exhaust samples (averaging 46 % versus 1 %) while somewhere in between (10–26 %) for Fresno and Reno wildfire samples. Effective α_{BrC} compares well among Fresno, Reno wildfire, and prescribed-burning samples (4.2–4.8) and is consistent with BrC of a similar nature from biomass burning (Bahadur et al., 2012; Kirchstetter and Thatcher, 2012). Even in the infrared region BrC accounts for 3, 6, and 24 % of $\tau_{a,980\ nm}$ for the Fresno, Reno, and prescribed-burning samples, respectively, on average. α_{BrC} in diesel exhaust, detectable in 5 of 11 samples, appears to be significantly lower (2.3 ± 0.1) than in other sample types.

Table 3 shows that BC_d as determined from $\tau_{a,635\ nm,BC}$ / $MAE_{635\ nm}$ ($7.4\ m^2\ g^{-1}$) are lower than $ECR_{635\ nm}$. The differences are especially significant (i.e., p value of RD < 0.01) for Reno wildfire and Tahoe prescribed-burning samples with relatively high BrC contributions. The comparisons do not change with $ECR_{808\ nm}$ (with low BrC influence) replacing $ECR_{635\ nm}$. A continuum of light-absorbing carbon from biomass burning – ranging from BrC and char to soot – as suggested by Pöschl (2003) and Masiello (2004) may explain the phenomenon. As char and soot resulting from pyrolysis and high-temperature graphitization, respectively, are both quantified as EC by TOA (Han et al., 2009), they may have distinct optical properties. BC_d that was calibrated against diesel EC would represent just the soot fraction because there is little char material in diesel exhaust. $ECT_{635\ nm}$ is substantially lower than $ECR_{635\ nm}$ due to the aforementioned POC effect and is much closer to BC_d for the Reno and Tahoe biomass burning samples but not the Fresno and diesel exhaust samples.

6 Conclusions

Thermal/optical analysis that combines thermal separation and optical monitoring is potentially a powerful tool for analyzing carbonaceous aerosol on filters. Spatiotemporal variations and long-term trends in aerosol loading, chemical composition, sources, and effects have been inferred from OC and EC measurements (e.g., Chen et al., 2012; Hand et al., 2012; Malm et al., 1994; Murphy et al., 2011; Park et al., 2006). As many archived samples may be retrieved for reanalysis and ∼40 000 new samples are collected per year in the US long-term networks alone, an enhanced multi-wavelength thermal/optical analyzer would benefit the scientific community that uses the data.

The seven-wavelength (visible to near-infrared regions) TSA with both R and T sensors allows the determination of the OC–EC split at different wavelengths and light absorption measurements to be made with wavelength-specific loading corrections. In the selected ambient and source $PM_{2.5}$ samples, contributions of BC and BrC to light absorption were decoupled, assuming an absorption Ångström

exponent of unity for BC and much higher values for BrC. Thus, BC concentrations optically equivalent to diesel exhaust EC, i.e., BC_d, can be calculated. BrC with an average absorption Ångström exponent of 4.2–4.8 is found to be enriched in samples influenced by biomass burning.

Despite the modifications in light source and detection technique, it is shown that the TSA measures $OC_{635\ nm}$ and $EC_{635\ nm}$ equivalent to $OC_{633\ nm}$ and $EC_{633\ nm}$ from conventional TOA following the same IMPROVE_A protocol with either R or T pyrolysis adjustment. $ECR_{635\ nm}$ is also consistent with those determined with longer wavelengths (e.g., 808 nm), though OC–EC splits with shorter wavelengths (e.g., 450 nm) increase ECR appreciably, showing the effect of BrC. For ECT, the BrC effect is somewhat canceled by an opposite POC effect. The optically derived BC_d underestimates $ECR_{635\ nm}$ or $ECR_{808\ nm}$ in biomass-burning-dominated samples with relatively high BrC content though the agreements are good for other samples. This discrepancy calls for further studies on the optical properties of EC, including soot and char, from biomass burning in contrast to those of diesel soot particles.

The Supplement related to this article is available online at doi:10.5194/amt-8-451-2015-supplement.

Acknowledgements. This work was supported, in part, by the US National Science Foundation (CHE 1214163), National Park Service IMPROVE Carbon Analysis Contract (C2350000894), and Chen's sabbatical leave at the University of Rostock. The authors thank Steve Kohl, Dana Trimble, and Gustavo Riggio at DRI for collection and carbon analysis of the samples and Megan Johnson for conducting the Lambda 35 spectral analysis. The conclusions are those of the authors and do not necessarily reflect the views of the sponsoring agencies.

Edited by: W. Maenhaut

References

Ahmed, T., Dutkiewicz, V. A., Shareef, A., Tuncel, G., Tuncel, S., and Husain, L.: Measurement of black carbon (BC) by an optical method and a thermal-optical method: Intercomparison for four sites, Atmos. Environ., 43, 6305–6311, 2009.

Andreae, M. O. and Gelencsér, A.: Black carbon or brown carbon? The nature of light-absorbing carbonaceous aerosols, Atmos. Chem. Phys., 6, 3131–3148, doi:10.5194/acp-6-3131-2006, 2006.

Arnott, W. P., Fujita, E. M., Walker, J., Campbell, D. E., Zielinska, B., Sagebiel, J. C., Moosmüller, H., Chow, J. C., and Lawson, D. R.: Photoacoustic Measurement of Black Carbon Emission Rates by Gasoline and Diesel Powered Vehicles and the Relationship with Carbon Analysis by Thermal Methods, in: Gasoline/Diesel PM Split Study: Source and Ambient Sampling, Chemical Analysis, and Apportionment Phase, prepared by Desert Research Institute, Reno, NV, Prepared for DOE National Renewable Energy Laboratory, 2–39, 2005a.

Arnott, W. P., Hamasha, K., Moosmüller, H., Sheridan, P. J., and Ogren, J. A.: Towards aerosol light-absorption measurements with a 7-wavelength Aethalometer: Evaluation with a photoacoustic instrument and 3-wavelength nephelometer, Aerosol Sci. Technol., 39, 17–29, 2005b.

Bahadur, R., Praveen, P. S., Xu, Y. Y., and Ramanathan, V.: Solar absorption by elemental and brown carbon determined from spectral observations, Proc. Natl. Acad. Sci. USA, 109, 17366–17371, 2012.

Birch, M. E. and Cary, R. A.: Elemental carbon-based method for occupational monitoring of particulate diesel exhaust: Methodology and exposure issues, Analyst, 121, 1183–1190, 1996.

Bond, T. C., Anderson, T. L., and Campbell, D. E.: Calibration and intercomparison of filter-based measurements of visible light absorption by aerosols, Aerosol Sci. Technol., 30, 582–600, 1999.

Bougiatioti, A., Zarmpas, P., Koulouri, E., Antoniou, M., Theodosi, C., Kouvarakis, G., Saarikoski, S., Makela, T., Hillamo, R., and Mihalopoulos, N., Organic, elemental and water-soluble organic carbon in size segregated aerosols, in the marine boundary layer of the Eastern Mediterranean, Atmos. Environ., 64, 251–262, 2013.

Cao, J. J., Lee, S. C., Chow, J. C., Watson, J. G., Ho, K. F., Zhang, R. J., Jin, Z. D., Shen, Z. X., Chen, G. C., Kang, Y. M., Zou, S. C., Zhang, L. Z., Qi, S. H., Dai, M. H., Cheng, Y., and Hu, K.: Spatial and seasonal distributions of carbonaceous aerosols over China, J. Geophys Res.-Atmos., 112, 1–9, 2007.

Cavalli, F., Viana, M., Yttri, K. E., Genberg, J., and Putaud, J.-P.: Toward a standardised thermal-optical protocol for measuring atmospheric organic and elemental carbon: the EUSAAR protocol, Atmos. Meas. Tech., 3, 79–89, doi:10.5194/amt-3-79-2010, 2010.

Chen, L.-W. A., Chow, J. C., Watson, J. G., Moosmüller, H., and Arnott, W. P.: Modeling reflectance and transmittance of quartz-fiber filter samples containing elemental carbon particles: Implications for thermal/optical analysis, J. Aerosol Sci., 35, 765–780, 2004.

Chen, L.-W. A., Watson, J. G., Chow, J. C., and Magliano, K. L.: Quantifying $PM_{2.5}$ source contributions for the San Joaquin Valley with multivariate receptor models, Environ. Sci. Technol., 41, 2818–2826, 2007.

Chen, L.-W. A., Chow, J. C., Watson, J. G., and Schichtel, B. A.: Consistency of long-term elemental carbon trends from thermal and optical measurements in the IMPROVE network, Atmos. Meas. Tech., 5, 2329–2338, doi:10.5194/amt-5-2329-2012, 2012.

Chen, L.-W. A., Han, Y. M., Chow, J. C., Watson, J. G., and Cao, J. J.: Black carbon in dust and geological material: Optical analysis and implication of urban influence, J. Aerosol Sci., submitted, 2015.

Chow, J. C., Watson, J. G., Pritchett, L. C., Pierson, W. R., Frazier, C. A., and Purcell, R. G.: The DRI Thermal/Optical Reflectance carbon analysis system: Description, evaluation and applications in U.S. air quality studies, Atmos. Environ., 27A, 1185–1201, 1993.

Chow, J. C., Watson, J. G., Crow, D., Lowenthal, D. H., and Merrifield, T. M.: Comparison of IMPROVE and NIOSH carbon measurements, Aerosol Sci. Technol., 34, 23–34, 2001.

Chow, J. C., Watson, J. G., Chen, L.-W. A., Arnott, W. P., Moosmüller, H., and Fung, K. K.: Equivalence of elemental carbon by Thermal/Optical Reflectance and Transmittance with different temperature protocols, Environ. Sci. Technol., 38, 4414–4422, 2004.

Chow, J. C., Watson, J. G., Chen, L.-W. A., Chang, M.-C. O., Robinson, N. F., Trimble, D. L., and Kohl, S. D.: The IMPROVE_A temperature protocol for thermal/optical carbon analysis: Maintaining consistency with a long-term database, J. Air Waste Manage. Assoc., 57, 1014–1023, 2007a.

Chow, J. C., Watson, J. G., Lowenthal, D. H., Chen, L.-W. A., Zielinska, B., Mazzoleni, L. R., and Magliano, K. L.: Evaluation of organic markers for chemical mass balance source apportionment at the Fresno supersite, Atmos. Chem. Phys., 7, 1741–1754, 2007b,
http://www.atmos-chem-phys.net/7/1741/2007/.

Chow, J. C., Watson, J. G., Doraiswamy, P., Chen, L.-W. A., Sodeman, D. A., Lowenthal, D. H., Park, K., Arnott, W. P., and Motallebi, N.: Aerosol light absorption, black carbon, and elemental carbon at the Fresno Supersite, California, Atmos. Res., 93, 874–887, 2009.

Chow, J. C., Watson, J. G., Chen, L.-W. A., Rice, J., and Frank, N. H.: Quantification of $PM_{2.5}$ organic carbon sampling artifacts in US networks, Atmos. Chem. Phys., 10, 5223–5239, doi:10.5194/acp-10-5223-2010, 2010.

Chow, J. C., Watson, J. G., Robles, J., Wang, X. L., Chen, L.-W. A., Trimble, D. L., Kohl, S. D., Tropp, R. J., and Fung, K. K.: Quality assurance and quality control for thermal/optical analysis of aerosol samples for organic and elemental carbon, Anal. Bioanal. Chem., 401, 3141–3152, 2011.

Clarke, A., McNaughton, C., Kapustin, V., Shinozuka, Y., Howell, S., Dibb, J., Zhou, J., Anderson, B., Brekhovskikh, V., Turner, H., and Pinkerton, M.: Biomass burning and pollution aerosol over North America: Organic components and their influence on spectral optical properties and humidification response, J. Geophys. Res.-Atmos., 112, D12S18, doi:10.1029/2006JD007777, 2007.

Dabek-Zlotorzynska, E., Dann, T. F., Martinelango, P. K., Celo, V., Brook, J. R., Mathieu, D., Ding, L. Y., and Austin, C. C.: Canadian National Air Pollution Surveillance (NAPS) $PM_{2.5}$ speciation program: Methodology and $PM_{2.5}$ chemical composition for the years 2003–2008, Atmos. Environ., 45, 673–686, 2011.

Favez, O., Cachier, H., Sciare, J., Sarda-Esteve, R., and Martinon, L.: Evidence for a significant contribution of wood burning aerosols to $PM_{2.5}$ during the winter season in Paris, France, Atmos. Environ., 43, 3640–3644, 2009.

Fujita, E. M., Zielinska, B., Campbell, D. E., Arnott, W. P., Sagebiel, J. C., Mazzoleni, L. R., Chow, J. C., Gabele, P. A., Crews, W., Snow, R., Clark, N. N., Wayne, W. S., and Lawson, D. R.: Variations in speciated emissions from spark-ignition and compression-ignition motor vehicles in California's south coast air basin, J. Air Waste Manage. Assoc., 57, 705–720, 2007.

Gorin, C. A., Collett Jr., J. L., and Herckes, P.: Wood smoke contribution to winter aerosol in Fresno, CA, J. Air Waste Manage. Assoc., 56, 1584–1590, 2006.

Hadley, O. L., Corrigan, C. E., and Kirchstetter, T. W.: Modified thermal-optical analysis using spectral absorption selectivity to distinguish black carbon from pyrolized organic carbon, Environ. Sci. Technol., 42, 8459–8464, 2008.

Han, Y. M., Lee, S. C., Cao, J. J., Ho, K. F., and An, Z. S.: Spatial distribution and seasonal variation of char-EC and soot-EC in the atmosphere over China, Atmos. Environ., 43, 6066–6073, 2009.

Han, Y. M., Chen, L.-W. A., Cao, J. J., Fung, K. K., Ho, K. F., Yan, B. Z., Zhan, C. L., Liu, S. X., Wei, C., and An, Z. H.: Thermal/optical methods for elemental carbon quantification in soils and urban dusts: Equivalence of different analysis protocols, Plos One, 8, e83462, doi:10.1371/journal.pone.0083462, 2013.

Hand, J. L., Schichtel, B. A., Pitchford, M. L., Malm, W. C., and Frank, N. H.: Seasonal composition of remote and urban fine particulate matter in the United States, J. Geophys Res.-Atmos., 117, D05209, doi:10.1029/2011JD017122, 2012.

Hansen, A. D. A., Rosen, H., and Novakov, T.: The aethalometer – An instrument for the real-time measurement of optical absorption by aerosol particles, Sci. Total Environ., 36, 191–196, 1984.

Huntzicker, J. J., Johnson, R. L., Shah, J. J., and Cary, R. A.: Analysis of organic and elemental carbon in ambient aerosols by a thermal-optical method, in: Particulate Carbon: Atmospheric Life Cycle, edited by: Wolff, G. T. and Klimisch, R. L., Plenum, New York, NY, USA, 79–88, 1982.

IMPROVE: Interagency Monitoring of Protected Visual Environments, prepared by National Park Service, Ft. Collins, CO, available at: http://vista.cira.colostate.edu/IMPROVE (last access: 16 January 2015), 2014.

Khan, B., Hays, M. D., Geron, C., and Jetter, J.: Differences in the OC/EC ratios that characterize ambient and source aerosols due to thermal-optical analysis, Aerosol Sci. Technol., 46, 127–137, 2012.

Kirchstetter, T. W. and Thatcher, T. L.: Contribution of organic carbon to wood smoke particulate matter absorption of solar radiation, Atmos. Chem. Phys., 12, 6067–6072, doi:10.5194/acp-12-6067-2012, 2012.

Lack, D. A., Moosmüller, H., McMeeking, G. R., Chakrabarty, R. K., and Baumgardner, D.: Characterizing elemental, equivalent black, and refractory black carbon aerosol particles: a review of techniques, their limitations and uncertainties, Anal. Bioanal. Chem., 406, 99–122, 2014.

Malamakal, T., Chen, L.-W. A., Wang, X. L., Green, M. C., Gronstal, S., Chow, J. C., and Watson, J. G.: Prescribed burn smoke impact in the Lake Tahoe Basin: model simulation and field verification, Int. J. Environ. Poll., 52, 225–243, 2013.

Malm, W. C., Sisler, J. F., Huffman, D., Eldred, R. A., and Cahill, T. A.: Spatial and seasonal trends in particle concentration and optical extinction in the United States, J. Geophys. Res., 99, 1347–1370, 1994.

Masiello, C. A.: New directions in black carbon organic geochemistry, Mar. Chem., 92, 201–213, 2004.

Moosmüller, H., Chakrabarty, R. K., and Arnott, W. P.: Aerosol light absorption and its measurement: A review, J. Quant. Spectrosc. Radiat. Transfer, 110, 844–878, 2009.

Murphy, D. M., Chow, J. C., Leibensperger, E. M., Malm, W. C., Pitchford, M., Schichtel, B. A., Watson, J. G., and White, W. H.: Decreases in elemental carbon and fine particle mass in the United States, Atmos. Chem. Phys., 11, 4679–4686, doi:10.5194/acp-11-4679-2011, 2011.

NIOSH: Method 5040 Issue 3 (Interim): Elemental carbon (diesel exhaust), in NIOSH Manual of Analytical Methods, 4th Edn.,

National Institute of Occupational Safety and Health, Cincinnati, OH, USA, 1999.

Park, R. J., Jacob, D. J., Kumar, N., and Yantosca, R. M.: Regional visibility statistics in the United States: Natural and transboundary pollution influences, and implications for the Regional Haze Rule, Atmos. Environ., 40, 5405–5423, 2006.

Peterson, M. R. and Richards, M. H.: Thermal-optical-transmittance analysis for organic, elemental, carbonate, total carbon, and OCX2 in PM2.5 by the EPA/NIOSH method, in: Proceedings, Symposium on Air Quality Measurement Methods and Technology-2002, edited by: Winegar, E. D. and Tropp, R. J., 83-1-83-19, Air & Waste Management Association, Pittsburgh, PA, USA, 2002.

Petzold, A. and Schönlinner, M.: Multi-angle absorption photometry – A new method for the measurement of aerosol light absorption and atmospheric black carbon, J. Aerosol Sci., 35, 421–441, 2004.

Petzold, A., Ogren, J. A., Fiebig, M., Laj, P., Li, S.-M., Baltensperger, U., Holzer-Popp, T., Kinne, S., Pappalardo, G., Sugimoto, N., Wehrli, C., Wiedensohler, A., and Zhang, X.-Y.: Recommendations for reporting "black carbon" measurements, Atmos. Chem. Phys., 13, 8365–8379, doi:10.5194/acp-13-8365-2013, 2013.

Pöschl, U.: Aerosol particle analysis: Challenges and progress, Anal. Bioanal. Chem., 375, 30–32, 2003.

Quincey, P. G., Butterfield, D., Green, D., Coyle, M., and Cape, C. N.: An evaluation of measurement methods for organic, elemental and black carbon in ambient air monitoring sites, Atmos. Environ., 43, 5085–5091, 2009.

Reisinger, P., Wonaschutz, A., Hitzenberger, R., Petzold, A., Bauer, H., Jankowski, N., Puxbaum, H., Chi, X., and Maenhaut, W.: Intercomparison of measurement techniques for black or elemental carbon under urban background conditions in wintertime: Influence of biomass combustion, Environ. Sci. Technol., 42, 884–889, 2008.

Sandradewi, J., Prevot, A. S. H., Szidat, S., Perron, N., Alfarra, M. R., Lanz, V. A., Weingartner, E., and Baltensperger, U.: Using aerosol light absorption measurements for the quantitative determination of wood burning and traffic emission contributions to particulate matter, Environ. Sci. Technol., 42, 3316–3323, 2008.

Schauer, J. J. and Cass, G. R.: Source apportionment of wintertime gas-phase and particle-phase air pollutants using organic compounds as tracers, Environ. Sci. Technol., 34, 1821–1832, 2000.

Schauer, J. J., Mader, B. T., Deminter, J. T., Heidemann, G., Bae, M. S., Seinfeld, J. H., Flagan, R. C., Cary, R. A., Smith, D., Huebert, B. J., Bertram, T., Howell, S., Kline, J. T., Quinn, P., Bates, T., Turpin, B. J., Lim, H. J., Yu, J. Z., Yang, H., and Keywood, M. D.: ACE-Asia intercomparison of a thermal-optical method for the determination of particle-phase organic and elemental carbon, Environ. Sci. Technol., 37, 993–1001, 2003.

Schmid, H. P., Laskus, L., Abraham, H. J., Baltensperger, U., Lavanchy, V. M. H., Bizjak, M., Burba, P., Cachier, H., Crow, D., Chow, J. C., Gnauk, T., Even, A., ten Brink, H. M., Giesen, K. P., Hitzenberger, R., Hueglin, C., Maenhaut, W., Pio, C. A., Puttock, J., Putaud, J. P., Toom-Sauntry, D., and Puxbaum, H.: Results of the "Carbon Conference" international aerosol carbon round robin test: Stage 1, Atmos. Environ., 35, 2111–2121, 2001.

Snyder, D. C. and Schauer, J. J.: An inter-comparison of two black carbon aerosol instruments and a semi-continuous elemental carbon instrument in the urban environment, Aerosol Sci. Technol., 41, 463–474, 2007.

Subramanian, R., Khlystov, A. Y., and Robinson, A. L.: Effect of peak inert-mode temperature on elemental carbon measured using thermal-optical analysis, Aerosol Sci. Technol., 40, 763–780, 2006.

Turpin, B. J., Cary, R. A., and Huntzicker, J. J.: An in-situ, time-resolved analyzer for aerosol organic and elemental carbon, Aerosol Sci. Technol., 12, 161–171, 1990.

U.S.EPA: Chemical speciation, prepared by U.S. Environmental Protection Agency, Research Triangle Park, NC, 2014.

Virkkula, A., Ahlquist, N. C., Covert, D. S., Arnott, W. P., Sheridan, P. J., Quinn, P. K., and Coffman, D. J.: Modification, calibration and a field test of an instrument for measuring light absorption by particles, Aerosol Sci. Technol., 39, 68–83, 2005.

Watson, J. G., Chow, J. C., Bowen, J. L., Lowenthal, D. H., Hering, S. V., Ouchida, P., and Oslund, W.: Air quality measurements from the Fresno Supersite, J. Air Waste Manage. Assoc., 50, 1321–1334, 2000.

Watson, J. G., Chow, J. C., and Chen, L.-W. A.: Summary of organic and elemental carbon/black carbon analysis methods and intercomparisons, Aerosol Air Quality Res., 5, 65–102, 2005.

Watson, J. G., Chow, J. C., Chen, L.-W. A., and Frank, N. H.: Methods to assess carbonaceous aerosol sampling artifacts for IMPROVE and other long-term networks, J. Air Waste Manage. Assoc., 59, 898–911, 2009.

Yang, H. and Yu, J. Z.: Uncertainties in charring correction in the analysis of elemental and organic carbon in atmospheric particles by thermal/optical methods, Environ. Sci. Technol., 36, 5199–5204, 2002.

Yang, M., Howell, S. G., Zhuang, J., and Huebert, B. J.: Attribution of aerosol light absorption to black carbon, brown carbon, and dust in China – interpretations of atmospheric measurements during EAST-AIRE, Atmos. Chem. Phys., 9, 2035–2050, doi:10.5194/acp-9-2035-2009, 2009.

Zhang, X. L., Lin, Y. H., Surratt, J. D., Zotter, P., Prevot, A. S. H., and Weber, R. J.: Light-absorbing soluble organic aerosol in Los Angeles and Atlanta: A contrast in secondary organic aerosol, Geophys. Res. Lett., 38, L21810, doi:10.1029/2011GL049385, 2011.

Zhang, X. Y., Wang, Y. Q., Niu, T., Zhang, X. C., Gong, S. L., Zhang, Y. M., and Sun, J. Y.: Atmospheric aerosol compositions in China: spatial/temporal variability, chemical signature, regional haze distribution and comparisons with global aerosols, Atmos. Chem. Phys., 12, 779–799, doi:10.5194/acp-12-779-2012, 2012.

Zhong, M. and Jang, M.: Light absorption coefficient measurement of SOA using a UV-Visible spectrometer connected with an integrating sphere, Atmos. Environ., 45, 4263–4271, 2011.